Journal of Non-Crystalline Solids 596 (2022) 121843

Contents lists available at ScienceDirect

Journal of Non-Crystalline Solids

journal homepage: www.elsevier.com/locate/jnoncrysol

A novel borate-based 45S5 Bioglass®: *In vitro* assessment in phosphate-buffered saline solution

N.N. Yusof [a,b,*], Siti Maisarah Aziz [c,*], F. Mohd Noor [a,*], S.N. Syed Yaacob [a], S. Hashim [a]

[a] Physics Department, Faculty of Science, Universiti Teknologi Malaysia, Johor Bahru, Johor 81310, Malaysia
[b] School of Physics, Universiti Sains Malaysia, USM, Penang 11800, Malaysia
[c] UniSZA Science and Medicine Foundation Centre, Universiti Sultan Zainal Abidin, Gong Badak Campus, Kuala Nerus, Terengganu 21300, Malaysia

ARTICLE INFO

Keywords:
Boron
Borate
ICP-OES
45S5 Bioglass
In vitro
PBS

ABSTRACT

A novel borate-based 45S5 Bioglass® has been formulated and synthesized using the melt-quenching method. The *in vitro* assessment was performed to determine the bioactivity of the glasses using phosphate buffer saline (PBS) as an immersion solution. The pH measurement is performed using a pH meter, while ion dissolution is quantified using Inductively coupled plasma atomic emission spectrometer (ICP-OES). The immersion of borate-containing glass exhibits pH closes to human body fluid (≈7.40). The (Ca/P) atomic ratio was calculated and its value increased (1.7–4.0) along with borate contents, indicating improved bioactivity. The alteration of glass structure after the *in vitro* test is inspected using attenuated total reflectance sensor–Fourier transform infrared spectrophotometer (ATR-FTIR) and Raman spectrometer. The 45S5 Bioglass that comprised 40–80% of borate showed the appearance of HPO_4^{2-} a vibration band which specifies the growth of hydroxyapatite (HPA) after the *in vitro* test. Relative to 45S5 Bioglass®, glass labeled $0.4B_2O_3$ displayed the highest potential of HPA growth (248%), while dissolving BO_3 and BO_4 units at 57.36 and 8.48%, respectively. The new formulation technique offers an alternative path to control the degradation behavior of 45S5 Bioglass® glass by modifying the ratio of borate constituent. The prepared glass may find its potential in soft-bone tissue engineering applications.

1. Introduction

Over a half-decade, borate/borosilicate based bioglasses (BGs) has attracted many researchers for soft tissue engineering application due to their modifiable degradation properties that are valuable for biological-related work [1–10]. Typically BGs support the proliferation and differentiation of bone cells due to their ability to form strong bonds between hard and soft tissue; in this case, refer to bones and muscle, respectively [7]. The term 'bioglass' is owned for its chemical interaction with a solution that mimics human blood plasma which subsequently led to the formation of hydroxyl-carbonate apatite (HCA) layer—close to bone minerals. In short, HCA is a succeeding product of amorphous calcium phosphate (CaP) layers that crystallize on top of the glass surface. Typically CaP formation takes place after the degradation of cation modifier and hydrolysis of Si—O—Si bonds [11]. Among silica-based bioglass, 45S5 with composition $45SiO_2$-$24.5Na_2O$-24.5-CaO-$6P_2O_5$ (mol%) is the most studied glass, known as the first generation of bioglass, synthesis by Professor Larry Hench in 1969 [12]. Since the discovery, different kinds of glass modifiers were substituted and incorporated into the chemical composition to tailor their properties according to the clinical demands, such as better chemical resistance, high mechanical strength and additional biological or therapeutic functions [13–15]. Now BGs has progressed to the third generation and is expected to stimulate particular responses in cells at the molecular level [16,17].

It is worth mentioning that the 45S5 BGs doped with B_2O_3 are potential as third-generation bioactive material. Inclusion of B_2O_3 may provide a wider glass-forming range, as mentioned controllable degradation rates [7], preventing devitrification [17] and can transform into porous three-dimensional scaffolds for tissue engineering [10]. It may assist angiogenesis and osteogenesis *in vivo* [17]. Calcium (Ca) and boron (B) ions coupling increase bone growth to heal wounds. Boron ion has a great catalytic effect in BGs and is non-toxic at small amounts when included below 50 ppm [18]. Usually, B_2O_3 appeared in four- or three-fold coordinated in BGs. Previous work reports that a low concentration of B_2O_3 inside BGs will form as [BO_4] structural units meanwhile its high concentration exists as [BO_3] units inside the glass. The presence of [BO_3] structural units within the glass is said to lead to

* Corresponding authors.
E-mail address: smaisarahaziz@unisza.edu.my (S.M. Aziz).

https://doi.org/10.1016/j.jnoncrysol.2022.121843
Received 11 May 2022; Received in revised form 1 August 2022; Accepted 3 August 2022
Available online 20 August 2022

Table 1
Glass code and its composition in molar fraction.

Glass code	(1-α)	SiO_2	CaO	Na_2O	P_2O_5	α	B_2O_3
$0.0B_2O_3$	1	0.45	0.245	0.245	0.06	0	0
$0.2B_2O_3$	0.8	0.36	0.196	0.196	0.048	0.2	0.2
$0.4B_2O_3$	0.6	0.27	0.147	0.147	0.036	0.4	0.4
$0.6B_2O_3$	0.4	0.18	0.098	0.098	0.024	0.6	0.6
$0.8B_2O_3$	0.2	0.09	0.049	0.049	0.012	0.8	0.8
$1.0B_2O_3$	0	0	0	0	0	1	1

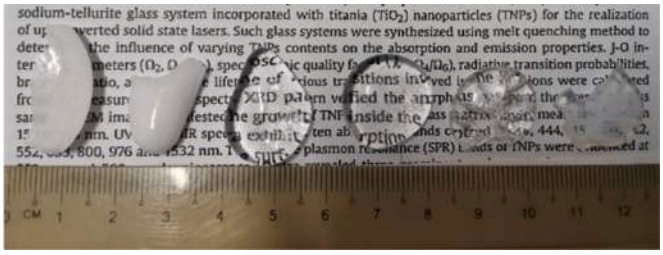

Fig. 1. Photograph of prepared glass. From left to right: $0.0B_2O_3$, $0.2B_2O_3$, $0.4B_2O_3$, $0.6B_2O_3$, $0.8B_2O_3$ and $1.0B_2O_3$, accordingly.

more linkages crossing between Si/P and B [7]. These linkages could alter the glass dissolution rate in a function of doping concentrations [7]. Thus, accessing the dynamic environment and degradation of 45S5 BGs at different B_2O_3 ratios could provide an additional understanding of compositional and structure relations in designing functional BGs.

Research in the past has focused on replacing SiO_2 as a backbone of 45S5 BGs with B_2O_3 or other modifiers, to cite a few [19–24]. Yet, a systematic study associated with the gradual replacement of overall 45S5 BGs constituent (SiO_2, Na_2O, CaO and $6P_2O_5$) with B_2O_3 has not been further explored. The dissolution properties of these glasses have not been completely understood, especially when immersed in human-like plasma; phosphate buffer saline (PBS). The dissolution of BO_3/BO_4 units responsible for formation of HPA has not been discussed. The composition−structure−dissolubility relationships of BGs has not been fully understood. Present glass examines the effect of substituting constituents of 45S5 BGs with B_2O_3 in terms of their bioactivity and structural properties. The samples prepared may be potential as customizable BGs for soft-tissue application.

2. Materials and methods

2.1. Samples preparation

The standard 45S5 Bioglass® (45S5 BGs) composition was modified by incorporating B_2O_3 proportionately into the formula [25]. The alteration of 45S5 BGs to borate (B_2O_3) ratio follow the composition: (1-α) $[45SiO_2\text{-}0.245Na_2O\text{-}0.245CaO\text{-}0.06P_2O_5]+\alpha B_2O_3$ where α is 0.0, 0.2, 0.4, 0.6, 0.8 and 1.0 in molar fraction. The glass formulation is summarized in Table 1. For each 15 g batch, high purity ≈99.9 of SiO_2, H_3BO_3, P_2O_5, $CaCO_3$ and Na_2CO_3 reagents from Sigma-Aldrich is placed into an alumina crucible and mixed thoroughly. All the raw constituent are in powder form and the code provided by Sigma-Aldrich for each constituent are as follows: SiO_2 (381276-99.9% purity), Na_2CO_3 (S2127-99.9% purity), $CaCO_3$ (239216-99.9% purity), B_2O_3 (289310-99.99% purity), P_2O_5 (214701-99.0% purity). The details about the reagents can be accessed via the codes provided by Sigma-Aldrich on their official website. The hygroscopic constituents such as P_2O_5 is placed last into the crucible to minimize any possible water contaminations. The mixture in the alumina crucible is heated at 10 °C/min from the room temperature to 1300 °C and held at melting temperature for 1 h. Subsequently, the melt is quenched by pouring it onto stainless steel at room temperature. The solidified glass is then kept inside a closed container to avoid unnecessary moisture attacks. Fig. 1 shows the photograph of as-prepared glasses. Note that glass viscosity, fragility, crystallization degree and forming ability largely depend on glass composition and the temperature at which these constituents are melted [26–28]. The change in viscosity may causes irregular shape of as-prepared glass once it is poured into stainless steel, especially some melt is left as residue inside the alumina crucible.

2.2. Characterization

2.2.1. Density and molar volume

The density of the glasses is measured by the Archimedes method using toluene as immersion where its density 0.8669 $g.cm^{-3}$. The measurement was taken three times and the mean and uncertainty is calculated. Density analysis acts as preliminary work to observe the

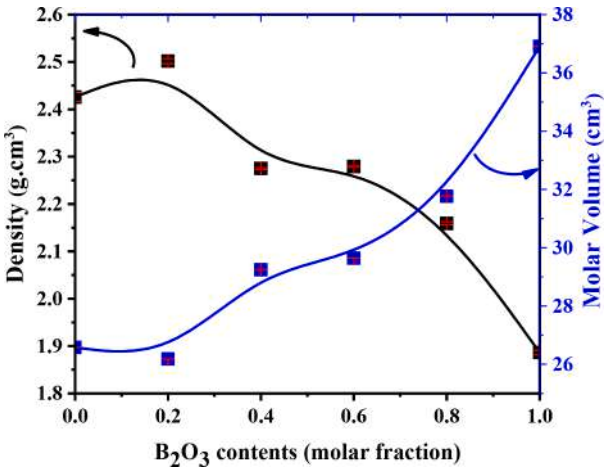

Fig. 2. Density and molar volume profile of prepared glass at different B_2O_3/45S5 BGs ratio.

Table 3
The value of density and molar volume of prepared glass.

Glass code	Molecular weight ($g.mol^{-1}$)	ρ ($g.cm^3$)	Δρ (g. cm^3)	M_v (cm^3. mol-1)	Δ M_v (cm^3.mol-1)
$0.0B_2O_3$	64.4764	2.426149	0.010	26.5756	0.004
$0.2B_2O_3$	65.5052	2.501946	0.005	26.1820	0.002
$0.4B_2O_3$	66.5340	2.275218	0.002	29.2429	0.001
$0.6B_2O_3$	67.5627	2.279259	0.002	29.6424	0.001
$0.8B_2O_3$	68.5915	2.158968	0.003	31.7705	0.002
$1.0B_2O_3$	69.6203	1.886116	0.005	36.9120	0.003

Table 2
Typical ion concentration within human blood plasma, SBF and PBS [29,30].

Solution	pH	Ion concentration (mM)							
		Na^+	K^+	Mg^{2+}	Ca^{2+}	Cl^-	HCO_3^-	HPO_4^{2-}	SO_4^{2-}
Blood Plasma	7.4	142.0	5.0	1.5	2.5	103	27	1.0	0.5
SBF	7.4	142	5.0	1.5	2.5	148.8	4.2	1.0	0.5
PBS	7.4	257.0	4.5	-	-	140.0	-	10.0	-

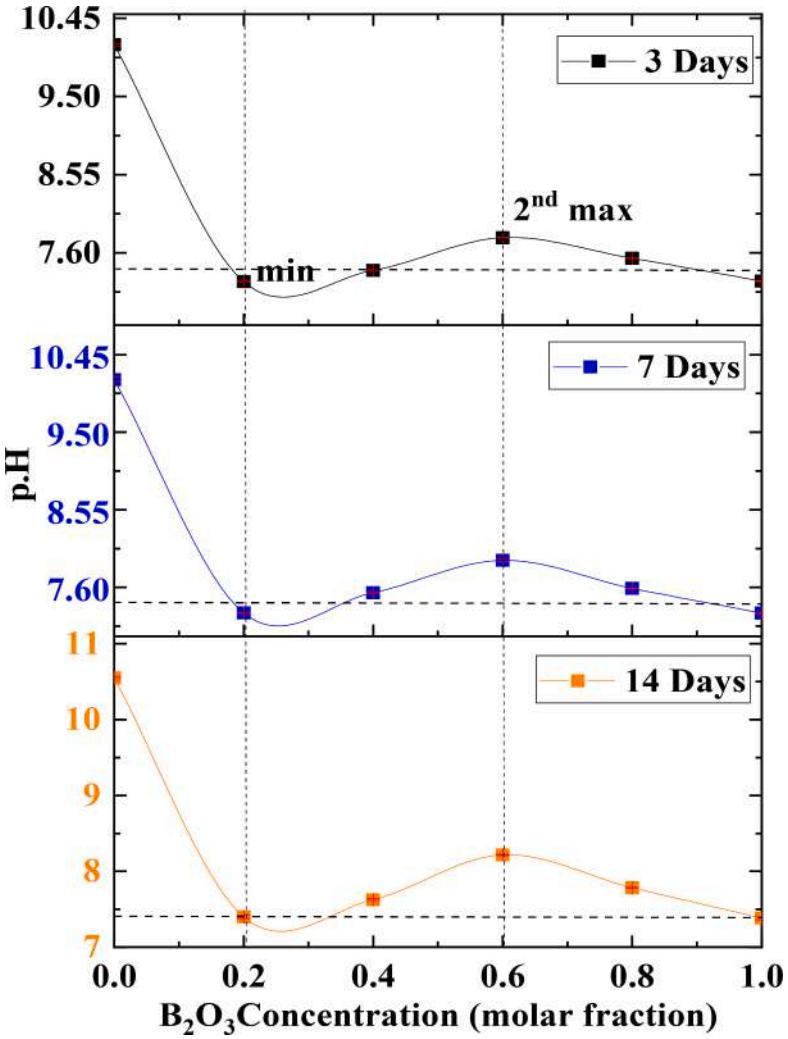

Fig. 3. The pH profile of sample dissolution as immersed in PBS at 3,7, 14 days.

possible anomaly behavior of B_2O_3 in 45S5 BGs.

2.2.2. *In vitro bioactivity tests*

The *in vitro* analysis assessment was performed to access the bioactivity and capability of the glass to form hydroxyapatite (HPA), $Ca_{10}(PO_4)_6(OH)_2$; a mineral that supports bone ingrowth and osseointegration. Phosphate buffer saline (PBS) from R&M at 0.1 M without further dilution is selected as an immersion solution due to its ease of handling compared to simulated body fluid (SBF). PBS contains ions and pH (≈7.4) close to human blood plasma (physiological solutions), except for the absence of Mg^{2+}, Ca^{2+} and HCO_3^- ions. Table 2 enlist the concentration of ions present in blood plasma, SBF and PBS. The fine powder (≈150 μm) of each sample was dispersed in PBS solution at a ratio of 1.5 mg/ml, placed in high-density polyethene (HDPE) plastic container before being held at temperature 37 °C for 3, 7, 14 days. The HDPE plastic container was used instead of the glass container to prevent the growth of apatite that may be caused by degradation of the glass container. After the dissolution process, the pH of each immersion contains a different ratio of 45S5 BGs/B_2O_3 is measured using pH meter (EUTECH Model PC2700). The elemental concentrations of [Si], [P] and [Ca] degraded from the sample are quantified using inductively coupled plasma optical emission spectroscopy (ICP-OES, Varian Liberty 150, Agilent Technologies). All measurements were performed in triplicates, where the mean, standard deviation and relative standard deviation is calculated.

Additional PBS immersion containing respective samples is prepared using the same procedure aforementioned, except the ratio of sample to PBS is set to 5 mg/ml. The second *in vitro* test is to examine any possible structure modification after the *in vitro* test. The previous set-up causes all the glass to dissolve into the solution. The precipitated powder is filtered, dried and characterised using an attenuated total reflectance sensor–Fourier transform infrared spectrophotometer (FTIR-UATR; Perkin Elmer Spectrum, model Frontier) and Raman Spectrophotometer (LabRAM HR Evolution model, Horiba). The possible growth of HPA is scrutinized through FTIR and Raman spectra.

3. Results and discussion

3.1. *Density and molar volume*

The density analysis may reveal possible anomaly behaviors of borate (B_2O_3) as integrated with 45S5 BGs. The B_2O_3 anomaly could impact the degree of glass connectivity which correlates with ion dissolution [31,32]. Fig. 2 illustrates the patterns of density (ρ) and molar volume (M_v) for 45S5 BGs at different B_2O_3 molar fractions (0.0–1.0). Table 3 tabulated the ρ and M_v values of studied glass. Overall, the results show the reduction of ρ values (2.43–1.89) $g.cm^3$ as a function of B_2O_3 molar fraction, except for sample 45S5 BGs containing 20% of B_2O_3. The results are consistent with a model reported by Vedishcheva wherein the ρ of sodium silicate-based glass in their studies decreases with B_2O_3 inclusion, but the claim is only valid when the molar fraction of B_2O_3 is above 0.2 [33]. Previous work also revealed a

Table 4
The pH reading of prepared glass in PBS (37 °C) at a different time interval (3, 7, 14 days), including their standard deviation (SD) and relative standard deviation (RSD%).

3 days						
Sample	pH reading					
	First	Second	Third	Mean	SD	RSD%
$0.0B_2O_3$	10.14	10.11	10.14	10.13	0.014	0.140
$0.2B_2O_3$	7.26	7.24	7.25	7.25	0.008	0.113
$0.4B_2O_3$	7.4	7.38	7.38	7.39	0.009	0.128
$0.6B_2O_3$	7.78	7.79	7.78	7.78	0.005	0.061
$0.8B_2O_3$	7.53	7.54	7.53	7.53	0.005	0.063
$1.0B_2O_3$	7.26	7.26	7.25	7.26	0.005	0.065
7 days						
Sample	pH reading					
	First	Second	Third	Mean	SD	RSD%
$0.0B_2O_3$	10.18	10.1	10.15	10.14	0.033	0.325
$0.2B_2O_3$	7.29	7.29	7.28	7.29	0.005	0.065
$0.4B_2O_3$	7.54	7.52	7.54	7.53	0.009	0.125
$0.6B_2O_3$	7.94	7.91	7.94	7.93	0.014	0.178
$0.8B_2O_3$	7.59	7.59	7.58	7.59	0.005	0.062
$1.0B_2O_3$	7.28	7.29	7.28	7.28	0.005	0.065
14 days						
Sample	pH reading					
	First	Second	Third	Mean	SD	RSD%
$0.0B_2O_3$	10.57	10.54	10.54	10.55	0.014	0.134
$0.2B_2O_3$	7.39	7.43	7.38	7.40	0.022	0.292
$0.4B_2O_3$	7.61	7.63	7.64	7.63	0.013	0.164
$0.6B_2O_3$	8.21	8.23	8.21	8.22	0.009	0.115
$0.8B_2O_3$	7.78	7.79	7.78	7.78	0.005	0.061
$1.0B_2O_3$	7.37	7.41	7.37	7.38	0.019	0.255

low density (2.04 g.cm^3) and refractive index (1.47) of sodium silicate-based glass as B_2O_3 is added to their sample [5,34] Thus, the present findings are in agreement with earlier studies. It is worth mentioning that the total molecular weight of pure borate glass (69.62 g) is heavier than pure 45S5 BGs (64.47 g). Thus, a decrease in ρ glasses is less likely caused by the light-weight of B_2O_3 constituent. It can be assumed that decline of ρ value may contribute to the shortening of glass linkages and a more open network structure [6]. This means the prepared glass becomes less compact with B_2O_3. Contrary, the molecular volume increases with B_2O_3 content indicating an increase of empty spaces (voids) within the network, thus, supporting the deduction. There are no obvious anomalies traits observed in the density patterns as a function of B_2O_3, except for glass coded $0.2B_2O_3$.

3.2. pH test

Fig. 3 illustrates the pH of PBS containing a different ratio of B_2O_3 to 45S5 BGs, set at 37.0 ± 0.1 °C for 3, 7 and 14 days. Meanwhile, Table 4 tabulated the pH value including the standard deviation (SD) and relative standard deviation (RSD%). A small SD (0.004–0.033) and RSD (0.061–0.325) confirmed the reliability of the data. The pH value shows the same trends in all time intervals and samples. Generally, the PBS pH is drastically reduced (become acidic) as B_2O_3 is incorporated into the glass. The solution immersed with 45S5 BGs with 20% of B_2O_3 displays the lowest pH value (7.39−7.26). However, as the ratio of B_2O_3 to 45S5 increased up to 60%, the pH value rose to 8.21 as observed on day 14. The fluctuation of pH value is attributed to the variation of boron acid derivatives from B_2O_3 hydrolysis [9]. Increasing pH after dissolution could indicate a high level of silanol (Si-OH) forming in the media [35]. It involves exchanges of Na^+/H^+ ions through a reaction $Si-O-Na^+ + H^+ + OH^- \rightarrow Si-OH^+ + Na^+(aq) + OH^-$ [36]. Nevertheless, other than the presence of boric acid derivative, the possible drop of pH could be attributed to the occurrence of calcium phosphates and carbonates precipitation through reaction: $HCO_3^- \leftrightarrow CO_3^{-2} + H^+$ and $HPO_3^{-2} \leftrightarrow PO_3^{-3} + H^+$ [36]. Although human body fluid is circulated within the body, the excessive increase of pH (become alkaline) from ions degradation would be a disadvantage in osteogenesis [37]. Thus, the replacement of some fraction of 45S5 BGs with B_2O_3 may be beneficial in adjusting the pH closed to human body fluids to help in promoting protein adsorption that is essential for bone cell adhesion, proliferation and mineralization regulations [38]. To inspect the possible formation of calcium phosphate precipitate as a precursor of hydroxyapatite ($Ca_5(PO_4)_3(OH)_2$), the Inductively Coupled Plasma-Optical Emission Spectroscopy (ICP-OES), Attenuated Total Reflection- Fourier Transform Infrared (ATR-FTIR) and Raman spectrometer is utilized.

3.3. Immersion in PBS studies: in vitro analysis

The possible formation of an amorphous calcium phosphate layer (ACP) and hydroxyapatite (HPA) in a physiological medium is predicted based on the bioactivity of the prepared glass in PBS. The bone-bonding ability *in vivo* is correlated with *in vitro* calcification of biomaterials. ICP-OES measurements were performed to oversee ion dissolution for *in vitro* analysis [39].

Since the trends of pH in the all-time interval (3, 7, 14 days) are synchronized, only the sample's immersion on day 14 is selected for ICP-OES measurement. The selection of the sample is based on its longest soaking period to allow ACP/HPA growth. The concentration of [Si], [P] and [Ca] that degrade from the samples are quantified and presented in Fig. 4. A value of offset P is the concentration of [P] element contributed from the degradation process of glass, excluding the quantities of phosphate measured from PBS solutions *in vitro*. Meanwhile, Table 5 tabulated the value of ion concentration dissolved from the samples. A high concentration of [Si] detected indicates the rapid glass dissolution, while the existence of [Ca] and [P] in solution reflects the ability of the glass to form a calcium phosphate layer for bone proliferation [29]. The [Si] concentration release from sample $0.0B_2O_3$ is the highest compared to the rest of the glass. The [Si] concentration reduced significantly when B_2O_3 were incorporated into 45S5 BGs. Previous work mentions that additional oxide such as NbO_6 could replace some part of SiO_2 tetrahedra in the glass network, creating Si—O—Nb bonds. This new bond could delay the dissolution of Si—O—Si bonds [40]. Previous leaching test on SiO_2−CaO sol-gel hybrid material with high content boron also shows a low release of [Si]. They claimed the Si ions form a bond with boron, thus making the Si less dissolved in the physiological fluids [18]. Similarly, in the present case, integrated B_2O_3 into 45S5 BGs may lead to low [Si] concentration dissolution due to the possible formation of Si—O—B bonds. Another possible reason is the reduction of SiO_2 constituents within the sample itself.

Results show a high concentration of [P] and [Ca] in $0.2B_2O_3$-immersion, that also exhibits low pH compared to borate-free PBs immersion. Dissolution of B_2O_3 in PBS increases H^+ contents and raises dissolution of [Ca] and [P] from the glass. In other words, an acidic solution improves the solubility of calcium phosphate [36]. It is known that ion dissolution is better in acidic solution (pH < 7.4) compare to physiological media [41]. Nevertheless, the concentration of [P] and [Ca] in $0.6B_2O_3$-immersion decreased despite the high contents of B_2O_3. Noted that the pH of $0.6B_2O_3$-immersion increased (become alkaline) relative to $0.2B_2O_3$-immersion. The possible creation of Si-O-B linkages in sample $0.6B_2O_3$ may lead to physical and structural change in the glass network and consequently influences the dissolution and degradation properties of the glass [2,23,42]. Other than that, the rapid release of alkali ions such as Na^+ and Ca^{2+} from B_2O_3 dissolution could raise the pH solution slightly, simultaneously with B_2O_3 degradation [43]. Another possibility is when ions such as [P] and [Ca] have precipitated into the calcium phosphate layer on top of a glass surface, decreasing their concentration in the solutions [18].

The ratio of (Ca/P) and (Ca/Si) values is demonstrated in Table 6. The calcium to phosphorus (Ca/P) atomic ratio determines the probability of the glass-forming ACP to HPA. The (Ca/P) atomic ratio is calculated by multiplying the ratio of [Ca]/[P] concentrations from an ICP-OES by ten [44]. An increase of (Ca/P) atomic ratio (1.7–4.0) along B_2O_3 contents indicates an increase in bioactivity [45]. A previous study

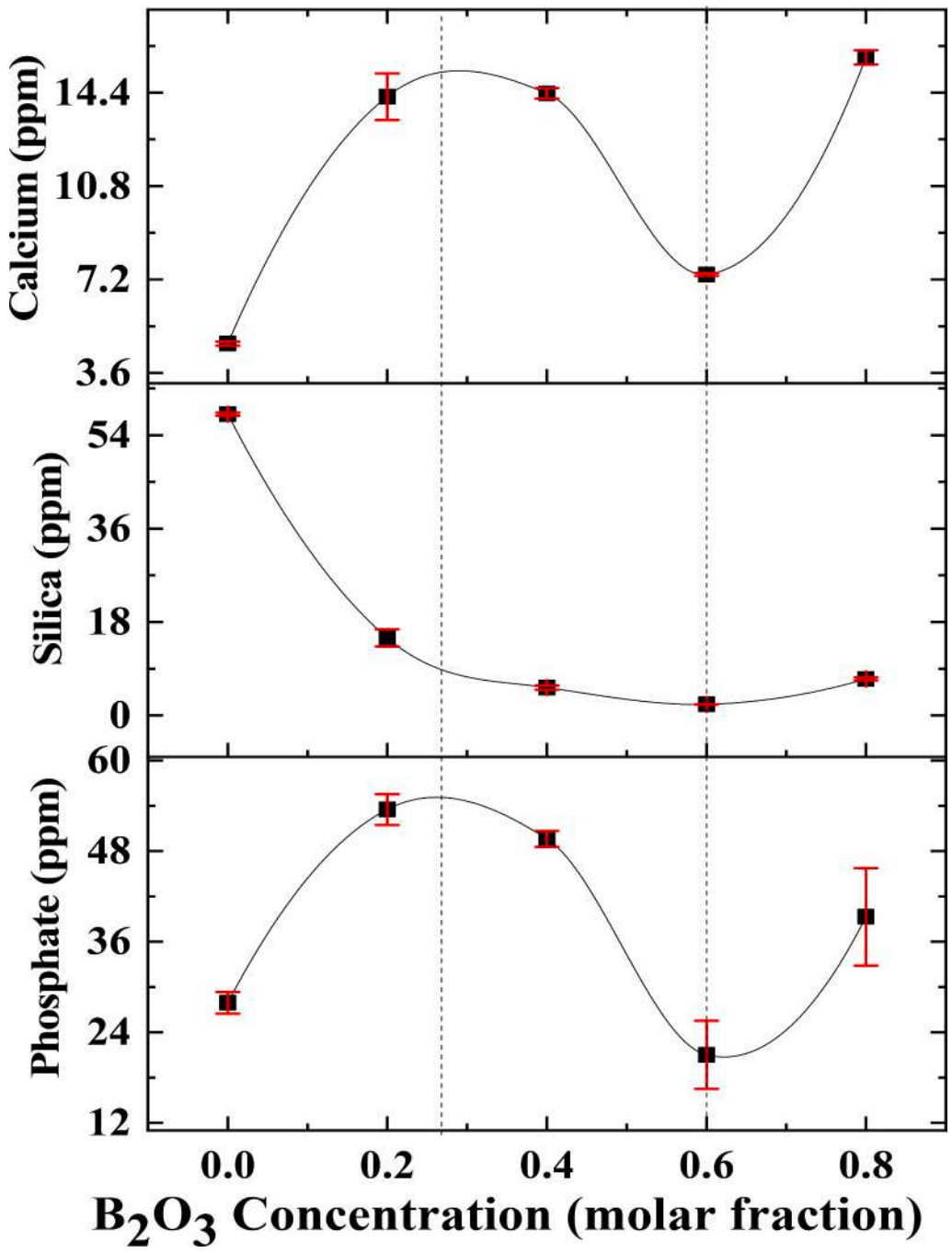

Fig. 4. Concentration profile of [Si], [P] and [Ca] degrade from samples after immersion in PBS for 14 days.

on 45S5 BGs containing B_2O_3 using different glass preparation has revealed improved growth of HPA with B_2O_3 inclusion [46]. Meanwhile, an increase of the (Ca/Si) ratio as function B_2O_3 in 45S5 BGs signifies the shortening of glass connectivity [47]. Therefore, when the (Ca/Si) ratio is higher, the network connectivity of the glass decrease. However, a decrement of (Ca/Si) ratio in sample $0.8B_2O_3$ indicates elongation of glass connectivity, unlike other glass series [45].

The dissolution precipitation process of B_2O_3-45S5 BGs follows a similar process as free-borate 45S5 BGs except for the absence of silica-rich amorphous precipitations [6]. The mechanism is systematically described by Hench in five steps [25]. Fig. 5 illustrates Hench's mechanism. In the first stage, the exchange reactions between the glass network modifiers (Na^+, Ca^{2+},) and H^+ (or H_3O^+) occur where silica (Si-O-Si) groups are hydrolyzed and formed silanol groups (Si-OH); through reaction$Si-O-Na^+ + H^+ \rightarrow Si-OH^+ + Na^+(aq)$[48]. Simultaneously, B_2O_3 within the glass may go hydrolysis through reaction $B_2O_3 + H_2O \rightarrow 2HBO_2$ and follow by$HBO_2 + H_2O \rightarrow B(OH)_3$ [20, 49]. This means that while Si—O—Si bonds degrade, the BO_3^{3-} ions are also released into the solutions during the *in vitro* test [21]. This claim was also supported by Abdelghany and Kamal as he mentioned B_2O_3-45S5 BGs dissolved by hydrolysis, hydration, and ion exchange reactions in an aqueous environment. The hydrolysis reactions and dissolution kinetics are responsible for controlling the degradation of B_2O_3-45S5 BGs [20,50]. This may explain the reduced pH value of PBS immersion when incorporated with B_2O_3-contained 45S5 BGs. The acidity from $B(OH)_3$ over $Si(OH)_4$ during glass degradation could slightly neutralise the alkaline solution [6,7]. The second stage proceeds as Si—O—Si bonds continue hydrolyzed to $Si(OH)_4$ through reaction

Table 5
Phosphorus, silicon and calcium ions concentrations that degrade from samples, include its SD and RSD%.

Phosphorus in ppm				
Sample	P	Offset P	SD	RSD%
$0.0B_2O_3$	323.9	27.9	1.43	0.44
$0.2B_2O_3$	349.5	53.5	2.04	0.58
$0.4B_2O_3$	345.6	49.6	1.06	0.31
$0.6B_2O_3$	317.0	21.0	4.51	1.42
$0.8B_2O_3$	335.3	39.3	6.45	1.92
Silicon in ppm				
Sample	Si		SD	RSD%
$0.0B_2O_3$	58.03		0.307	0.53
$0.2B_2O_3$	14.95		1.630	10.90
$0.4B_2O_3$	5.379		0.428	7.95
$0.6B_2O_3$	2.124		0.029	1.35
$0.8B_2O_3$	7.025		0.300	4.27
Calcium in ppm				
Sample	Ca		SD	RSD%
$0.0B_2O_3$	4.730		0.077	1.62
$0.2B_2O_3$	14.24		0.899	6.31
$0.4B_2O_3$	14.37		0.201	1.40
$0.6B_2O_3$	7.394		0.054	0.73
$0.8B_2O_3$	15.76		0.279	1.77

Table 6
The ratio of (Ca/P) and (Ca/Si) dissolved in PBS immersion. The dissolution rate (ppm/day) is included.

Sample	Ratio Ca/P	Ratio Ca/Si	Dissolution rate(ppm/day)		
			P	Si	Ca
$0.0B_2O_3$	1.7	0.08	0.026	0.015	0.002
$0.2B_2O_3$	2.7	0.95	0.064	0.005	0.006
$0.4B_2O_3$	2.9	2.67	0.081	0.002	0.008
$0.6B_2O_3$	3.5	3.48	0.052	0.001	0.007
$0.8B_2O_3$	4.0	2.24	0.198	0.010	0.028

$Si-O-Si + H_2O \rightarrow Si-OH + OH-Si$. The third stage involved condensation and polymerization of the amorphous gel-like SiO_2 layer. In the fourth stage, ions such as Ca^{2+} and $(PO_4)^{3+}$ adsorb on top of sol-gel SiO_2 precipitation and formed the ACP layer. Subsequently in the final stage, the ACP layer crystalized while also incorporating ions such as $(OH)^-$ and a small amount of $(CO_3)^{2-}$ to form the HPA/HCA layer [46,48].

Glass comprised of high borate contents permits the rapid release of alkali ions (Na^+, Ca^{2+}) due to easy breakage of B-O-B chains [2]. It is worth noting that the main structure of borate glasses is comprised of BO_3 trihedron that is unable to form into a three-dimensional network structure which led to low cross-linking density. This occurrence allows PBS to degrade the glass faster compared to glass comprised of high Si-O-Si linkages [51]. The dissolution-precipitation reactions occur continuously until all soluble parts of borate glass had dissolved [2]. The dissolution rate of the glass for each element in PBS is estimated using equation [52,53]

$$D_R(ppm/day) = \left(\frac{C_i - C_o}{C_s}\right) \times \left(\frac{1}{T}\right) \quad (1)$$

Where C_i is the concentration of the element obtained from ICP-OES, $C_o$is background concentration. The C_s is the concentration of the respective element in PBS immersion. Meanwhile $T$is the period of the *in vitro* test; in this case 14 days. The sample coded $0.8B_2O_3$ shows the fastest dissolution rate of elements P and Ca at 0.198 and 0.028 ppm/day, except for Si, which dissolves at 0.010 ppm/day. However, increasing the dissolution rate may not necessarily lead to the highest HPA formation due to lacks of nucleation sites for bone proliferation [39]. Further analysis is required to inspect HPA formation.

3.4. ATR-FTIR

The ATR-FTIR spectra of glasses with different molar fractions of B_2O_3 before and after *in vitro* are shown in Fig. 6 and Fig. 7, respectively. Generally, the ATR-FTIR profile of the glass before and after the *in vitro* test shows almost similar patterns except for significant changes in bands around 1018 and 1400 cm^{-1}. The vibration bands that correspond to particular groups are predicted based on previous literature. Due to the overlapping of vibration bonds of almost the same frequency, it is almost impossible to distinguish each band by deconvolution technique [36].

The band around 674–705 cm^{-1} could be assigned to the symmetric stretching mode of Si—C bonds which may also be overlapped with the bending vibration of Si—O—B bonds—if B_2O_3 were incorporated into the glass composition [18,42]. Meanwhile, vibration band 772–784 cm^{-1} indicates the presence of bending vibration of B-O-B in BO_3. The shoulder peak around 885–878 cm^{-1} is characterized as B-O stretching of boroxol rings meanwhile broad band in the range 918–1200 cm^{-1} disclosed B-O linkages of BO_4 [22]. However, the band in the range 981–1018 cm^{-1} could be associated with Si—O—Si and P—O—P bonds as well, which are greatly affected after immersion [36,39]. The incorporation of B_2O_3 into glass may lead to a cross-linking between the phosphate and silica chains through the formation of P—O—B bonds and Si—O—B [54]. The asymmetric stretching of Si-O-NBO is positioned around 900–970 cm^{-1} [6,19,39,55]. There is a high chance that Si—O—NBO bonded with BO_4 units and raised the stretching frequency of Si-O-B around 925 cm^{-1} [56,57]. A strong band change around 1005–1052 cm^{-1} is allotted to the symmetric stretching mode of Si—O—Si bonds. The asymmetric bending vibration of CH_3 in $Si(CH_3)_2$ is located around 1403–1465 cm^{-1} [18].

The bands around 875–981 cm^{-1} may be attributed to the bending vibration of PO_4^{3-}bonds that are possibly converted toH_3PO_4 [58,59]. The defined and sharp center around 1022 cm^{-1} could also be ascribed to asymmetric stretching of PO_4^{3-}groups; a sign of crystalline phosphate surface layer formation [60]. The degradation of B_2O_3 converted them into $B(OH)_3$ or $B(OH)_4^-$. This breaks the glass network and allowed CO_3^{2-}, PO_4^{3-}, Ca^{2+}andOH^- ions in PBS to form carbonate and phosphate precipitates [61]. Despite precautions adopted, the carbonate groups (CO_3^{2-}) also could be contaminated in the glass network whenever in contact with the atmosphere. Their bending vibration bond may appear around 870 cm^{-1} [55] meanwhile their stretching mode could be located around 1410 and 1458 cm^{-1} [58,62,63]. These bands could be overlapped BO_3 units vibration bonds around 1314–1413 cm^{-1} which hardly distinguished from the functional groups [6,7,22,64]. Without comparing with sample $0.0B_2O_3$, the band about 1018 cm^{-1} becomes sharper as the molar fraction of B_2O_3 within the glass increased. This condition indicates a steady rise in bioactivity and controlled growth of the HPA layer [6].

Following Hench's dissolution processes, the reaction CO_3^{2-} with ACP allowed the growth of B-type carbonate apatite precipitation, $Ca_9(HPO_4)_{0.5}$ $(CO_3)_{0.5}(PO_4)_5OH$ (HCA), mimicking bone-like apatite [60]. Typical water (OH^-) bonds is evidenced about 1644 cm^{-1} and 3400 cm^{-1}, respectively [65]. These bands correspond to bending and symmetric stretching vibration mode, accordingly. Hydroxyl groups are involved in the formation of HPA via reaction $10Ca^{2+} + 6PO_{3-}^4 + 2OH^- \rightarrow Ca_{10}(PO_4)_6(OH)_2$[66]. In summary, sample $0.0B_2O_3$ is assumed to experience the highest dissolution of Si—O—Si bonds as reflected by the deep FTIR band around 1080 cm^{-1}. However, 45S5 BGs containing B_2O_3 seem to increase the deposition of PO_4^{3-} ions to form HPA. This assumption is supported by a sharp band around 1022–1052 cm^{-1} revealed by sample $1.0B_2O_3$ even in absence of SiO_2 bonds. Nevertheless, FTIR measurement is suspected unable to probe some vibration BO_3/BO_4^- bonds, thus Raman measurements were performed to support the study.

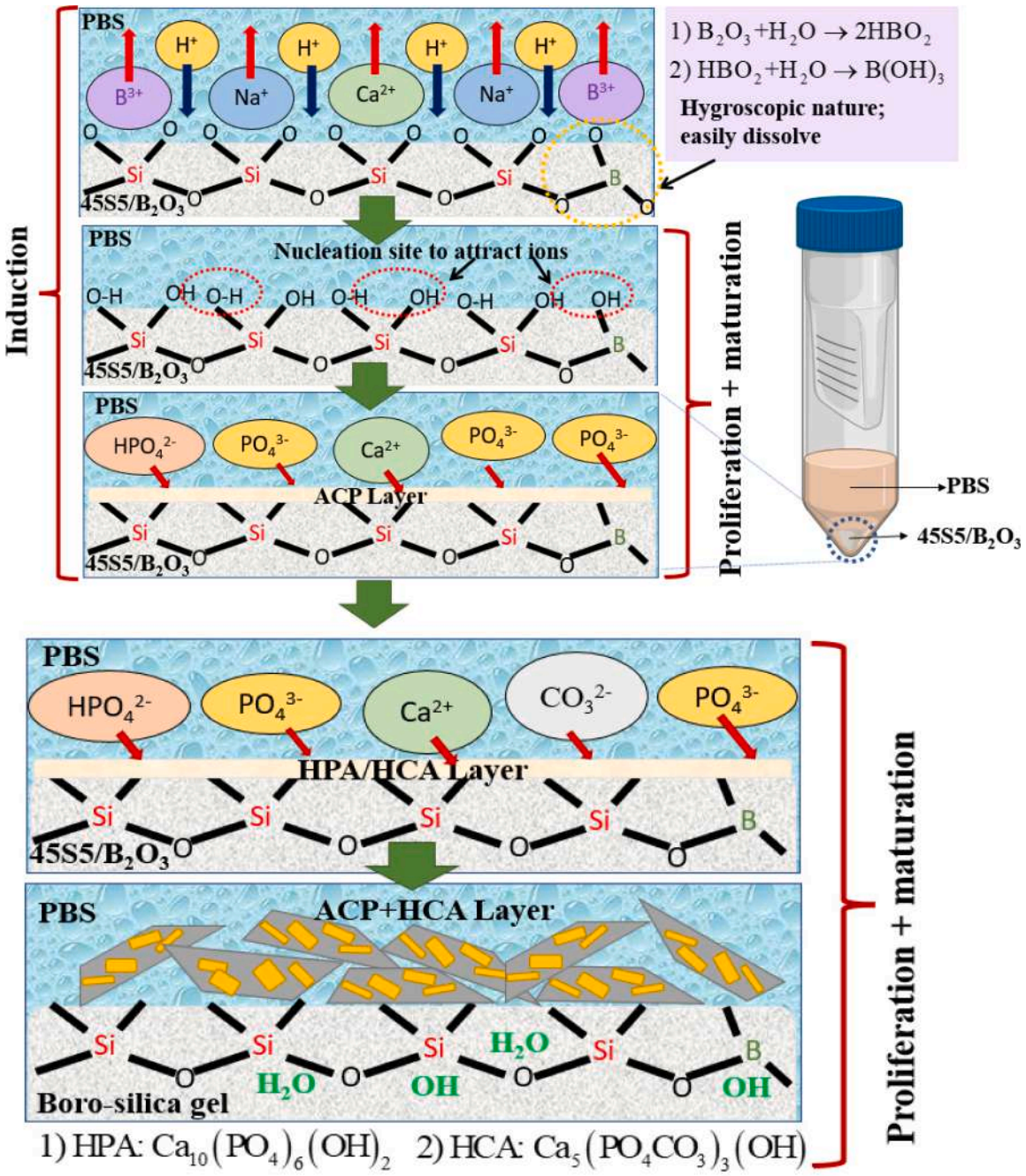

Fig. 5. Illustration of glass dissolution in PBS.

3.5. Raman

Raman analysis complements FTIR studies since some vibration modes are inactive in FTIR. Fig. 8 shows Raman spectra of glasses before an *in vitro* test, where Fig. 8(a) represent samples with a high 45S5 BGs to B_2O_3 ratio and Fig. 8(b) displayed represents glasses with high B_2O_3 to 45S5 BGs ratio. Here, free borate-45S5 BGs displayed prominent peaks around 425, 580, 965 and 1023 cm^{-1} which were assigned to bending vibration of O-Si-O, vibration at three/six-membered ring of Si—O bond, asymmetric stretching of Si-O-Si in Q_1 and Q_2 units, and asymmetric stretching of Si-O-Si in Q_3 units. Here Q_1, Q_2, Q_3 of Si-O-Si units refer to SiO_7^{6-}, SiO_6^{4-}, SiO_5^{2-}species having three, two, and one non-bridging oxygen (NBOs) [67,68]. As the ratio of B_2O_3 gradually increases to 20%, the vibration band within 45S5 BGs shifted to higher wavenumbers and the band around 965 and 1023 cm^{-1} seems to overlap and become broad. On other hand, the addition of B_2O_3 up to 40% has shifted the wavenumber to a higher frequency and revealed some hidden peaks around 488, 728 and 801 cm^{-1}. The broader band indicates Si—O—Si bonds distortion due to changes in bond length and angle; thus raising various Q_n units to represent Si—O bonds [5]. The hidden peaks aforementioned around 488, 728 and 801 cm^{-1} correspond to the vibration of BO_4 isolated tetrahedra/diborate groups[69], bending vibration in BO_3 units and lastly B-O stretching of boroxol rings [22]. Meanwhile, for 45S5 BGs with a high ratio of B_2O_3 (60, 80, 100%), the broad absorbance around 1023–1045 cm^{-1} indicates a decrease in stretching of Si-O-Si in Q_3 units, creation of BO_4 groups within the samples and creation of HPO_4^{2-} units. Increase absorbance around 805 cm^{-1} with B_2O_3 concentration indicated stronger vibration of oxygen atom within boroxol rings $(B_3O_6)^{3-}$, which also means BO_4 groups are consumed by BO_3 dependent on B_2O_3 contents. Vibration bonds around

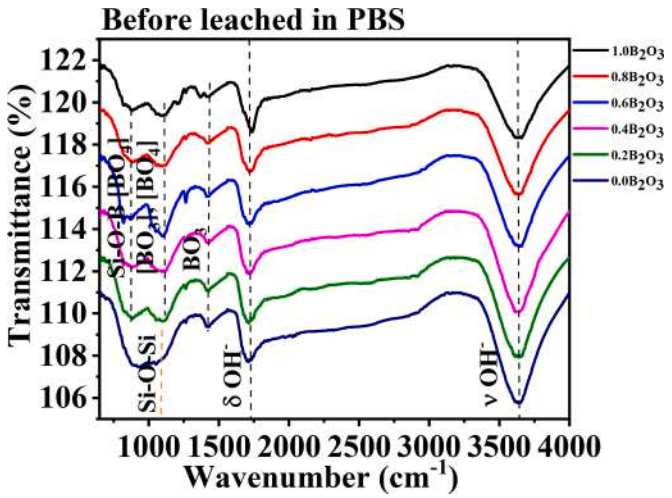

Fig. 6. ATR-FTIR spectra of the glass sample before *in vitro* test.

500 and 880 cm^{-1} represent the regeneration of BO_4 units in pentaborate, tetraborate and diborate groups [7,20].

Fig. 9 shows Raman spectra of glasses after the *in vitro* test. Meanwhile, Fig. 10(a)–(f) portrayed the structure modification of the glasses before and after the *in vitro* test. The 45S5 BGs made of 0.0–0.2 molar fraction of B_2O_3 show no significant difference in vibration bond. However, it is not the case for glass comprised 40–80% of B_2O_3. Their vibration band around 800 cm^{-1}, allocated to B-O stretching of boroxol rings is significantly reduced. This occurrence signifies the dissolution of glass at a high B_2O_3 ratio of over 40%. The new band around 507–567 cm^{-1} ascribed to P-O bending mode in PO_4^{3-} groups, revealing the formation of hydroxyapatite [70]. Meanwhile, the appearance of broadband around 1007–1087 cm^{-1} is allotted to asymmetric stretching of PO_4^{3-} groups which signifies the formation of crystalline surface layers of phosphates [60]. Raise band around 1300–1500 cm^{-1}, center around 1439 cm^{-1} indicates existence of carbonated hydroxyapatite (HCA) [71]. The previously mentioned twin band about 1420 and 1470 cm^{-1} is assigned to the asymmetric C-O stretching vibration of the CO_3^{2-} groups in carbonate apatite [70]. The band shift of 1439 cm^{-1} towards 1500 cm^{-1} indicates the conversion of apatite type where partially carbonated B hydroxyapatite turns to AB apatite [71]. Results suggest that the ratio of B_2O_3 above 0.2 of molar fraction haste the HPA growth.

Recognizing the coordination number of Boron (B) within the network provides insight into their role in creating the HPA layer. The coordination number here refers to the number of ligands that are attached to the central atom or ions, which in this case the central atom is Boron (B). For pure borate glass, BO_3 components are largely anticipated within the network in boroxol rings, allocated around 800 cm^{-1}. However, in a system with multicomponent oxide constituent, BO_3 groups are likely converted into BO_4 which mainly exist as diborate, triborate or pentaborate structures. Table 7 shows the predicted percentage of BO_3 and BO_4 units dissolve after the *in vitro* test for selected samples ($0.4B_2O_3$, $0.6B_2O_3$, $0.8B_2O_3$ and $1.0B_2O_3$). The sample was selected based on a significant change in Raman spectra after the *in vitro* assessment. The estimated percentage is calculated based on the bands area under the curve in the range 431–917 cm^{-1} using deconvulation technique [72]. Here, band around 431–455 cm^{-1} and 873–917 cm^{-1} is assigned as diborate, pentaborate and tetraborate groups [7] and bands around 778–810 cm^{-1} are approved as boroxol units [73]. The band 917 and 800 cm^{-1} shift to 873 and 778 cm^{-1} signify the conversion of borate linkages into $B(OH)_3$ and $B(OH)_4^-$ species after *in vitro* test [73]. In view of the high overlapping frequencies of Si—O, P—O, and B—O bonds in 1000–1400 cm^{-1}, the BO_4 and BO_3 groups are estimated in lower frequency ranges (430–950 cm^{-1}). Results show that BO_3 groups degrade faster than BO_4 sites. Thus, this explains the disappearance of boroxol peaks (mainly containing BO_3 units) around 800 cm^{-1} for glass coded $1.0B_2O_3$ [1,72]. The remaining B—O bonds are presumably associated with BO_4 species attached to hydrated silica network [1]. Table 8 enlisted the area under 1000–1033 cm^{-1} which is assigned to HPO_4^{2-} vibration bond, a precursor for HPA growth. After the *in vitro* assessment, sample $0.4B_2O_3$ demonstrated the highest percentage of potential HPA growth relative to 45S5 BGs (248%), by dissolving BO_3 and BO_4 at 57.36 and 8.48%, respectively; as shown in Fig. 11. The respective sample could be potential in soft-bone tissue engineering applications.

4. Conclusions

A series of glass composition (1-α) [$0.45SiO_2$-$0.245Na_2O$-$0.245CaO$-$0.06P_2O_5$]+αB_2O_3 where α is 0.0, 0.2, 0.4, 0.6, 0.8 and 1.0 in molar fraction were successfully prepared. The *in vitro* assessment revealed a drastic reduction of pH value (acidic nature) due to rapid hydrolysis of B_2O_3 from glass, inducing variation of boron acid derivates. PBS immersed with sample coded $0.06B_2O_3$ revealed a slight increase of pH, likely due to increasing migration of Na^+ and Ca^{2+} ions into solution; allowing OH production. The increase in (Ca/P) atomic ratio (1.7–4.0) along with B_2O_3 contents indicates increased of bioactivity. The sharp FTIR band around 1022 cm^{-1} for free borate-45S5 BGs and pure borate glass after the *in vitro* test exemplifies a fast phosphate crystal growth. For Raman analysis, a significant change in glass structure is evidenced for glass incorporated with a high B_2O_3 ratio (> 40%) after the *in vitro* test. The appearance of new bands around 1007–1087 cm^{-1} for 45S5 BGs integrated with 40–80% of B_2O_3 signifies an increase in HPA growth. The glass labeled $0.4B_2O_3$ glass displayed the highest potential

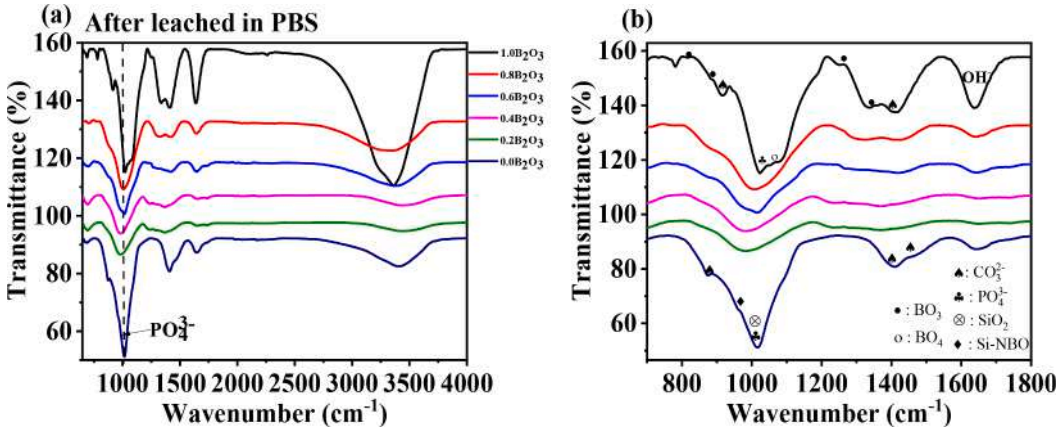

Fig. 7. (a) FTIR spectra of glass sample after immersed in PBS for 14 days in the range 650–400 cm^{-1} (b) 650–1800 cm^{-1}.

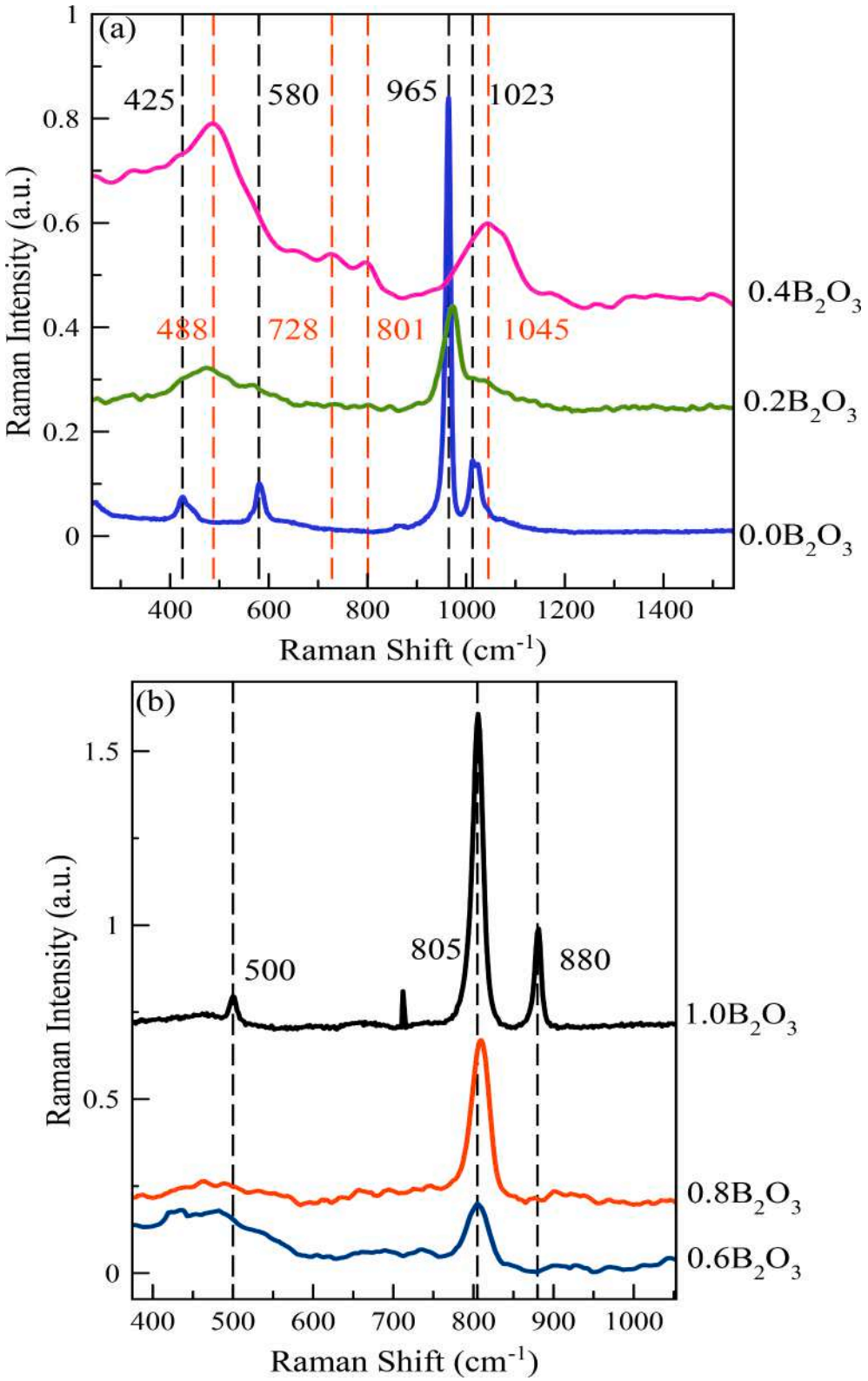

Fig. 8. Raman spectra for glasses with molar fraction of B_2O_3 at (a) 0.0–0.4 (b) 0.6–1.0 before *in vitro* test.

of hydroxyapatite formation (248%) while dissolving BO_3 units at 57.36 and 8.48% for BO_4 units. Results suggest that HPA formation could be controlled by tailoring the B_2O_3 ratios in 45S5 BGs. This new formulated glass may find its application in bone grafting and bioactive coatings by manipulating the degree of HPA formation to facilitate mineralization and protein adsorption onto bone tissue. *In vitro* tests on cytotoxicity and cytocompatibility of the glass could be done to ensure its safety as an implant material. A comprehensive evaluation on their fragility, crystallization kinetics and phase assemblage could be conducted to assess their ability to be moulded as bone scaffold.

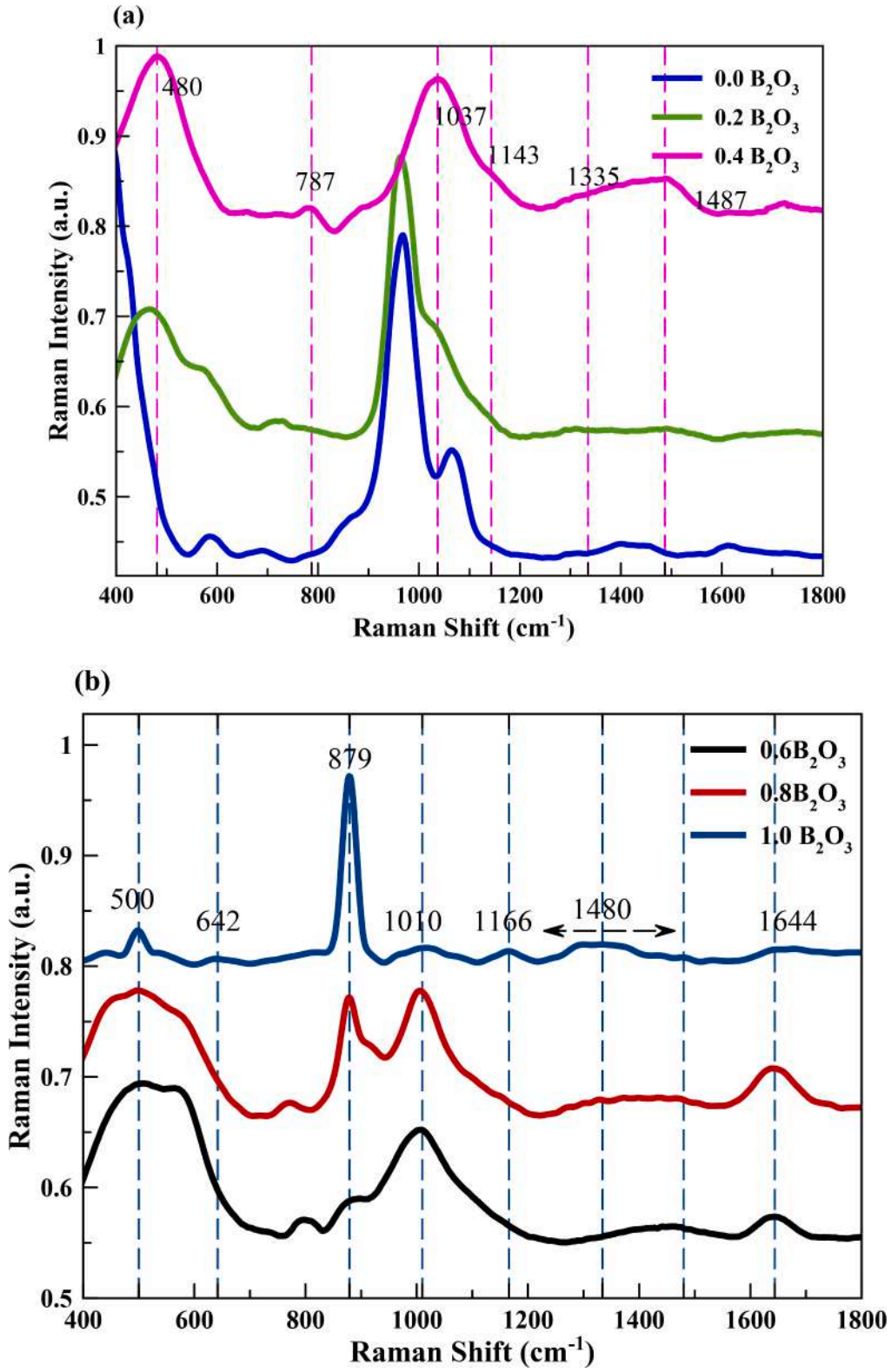

Fig. 9. Raman spectra for glasses with molar fraction of B_2O_3 at (a) 0.0–0.4 (b) 0.6–1.0 after *in vitro* test.

Author statement

The manuscript entitled **'A novel borate-based 45S5 Bioglass®: *in vitro* assessment in phosphate-buffered saline solution'** is original research work and has not been submitted /published in any journal. All authors have seen and approved the manuscript and have contributed significantly to the paper. The paper has been revised and agree for submission.

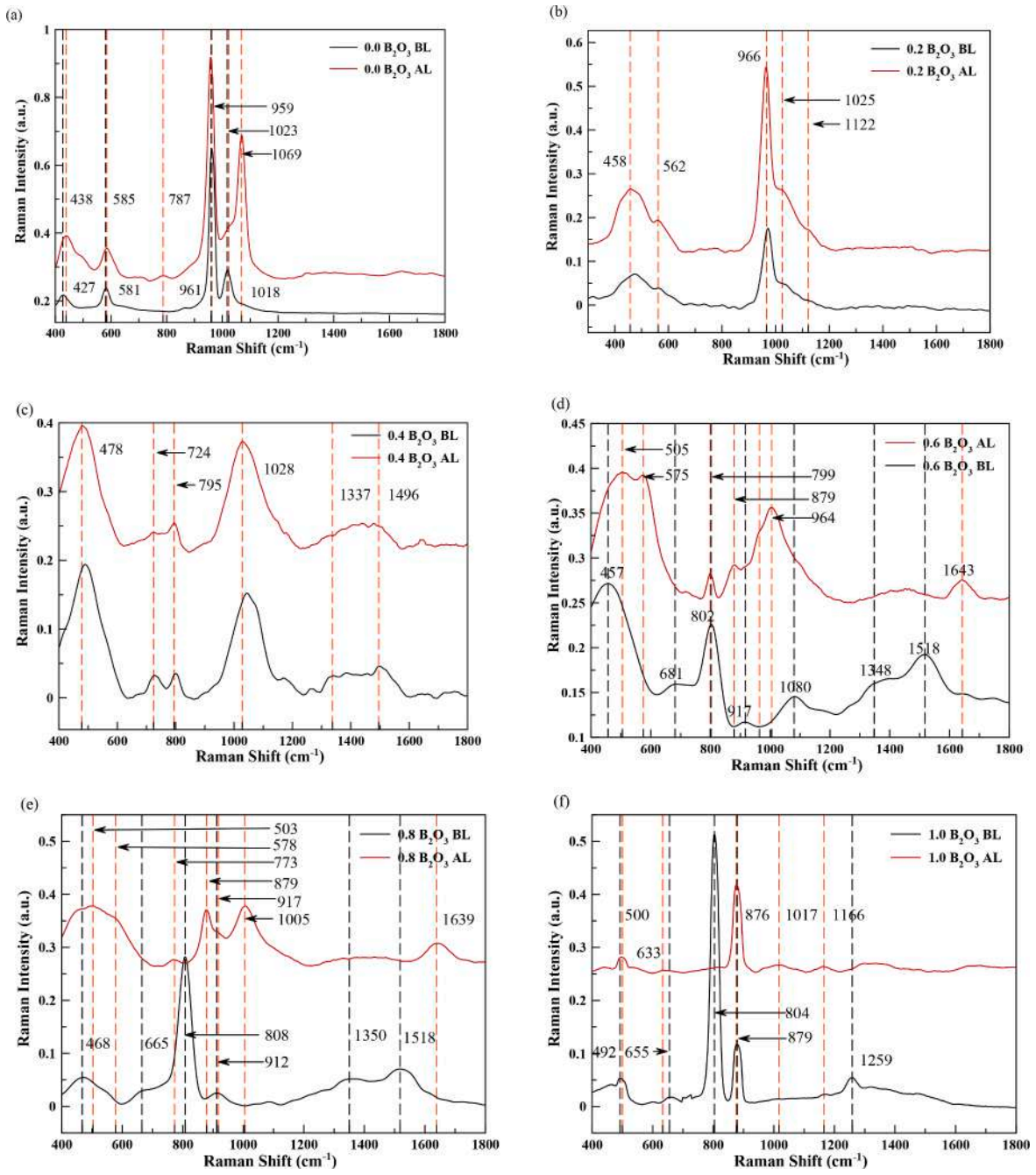

Fig. 10. (a)–(f) Raman spectra of prepared samples before (BL) and after *in vitro* test (AL).

Table 7
The area represents BO_3 and $(BO_4)^{-1}$ units within the samples and the percentage of BO_3 and $(BO_4)^{-1}$ dissolved in PBS.

Sample		Before *in vitro* test			After *in vitro* test			The dissolved BO_3 unit (%)	The dissolved $(BO_4)^{-1}$ unit (%)
$0.4B_2O_3$	Wavenumber (cm^{-1})	490	799	978	466	788	871	57.36	8.48
	Area	25.81	1.39	5.40	27.03	0.84	1.53		
$0.6B_2O_3$	Wavenumber (cm^{-1})	455	802	917	471	799	873	59.34	50.62
	Area	35.53	7.46	1.26	17.14	0.89	1.02		
$0.8B_2O_3$	Wavenumber (cm^{-1})	465	810	917	431	778	879	59.35	30.19
	Area	5.85	13.91	2.32	0.88	0.79	4.82		
$1.0B_2O_3$	Wavenumber (cm^{-1})	455	804	881	441	807	879	69.54	44.72
	Area	5.06	18.15	4.18	0.85	0.01	4.25		

Table 8
The area representing HPO_4^{2-} species that prerequisite for HPA growth after *in vitro* test.

Sample		After *in vitro* test	Potential HPA growth relative to 45S5 BGs (%)
$0.0B_2O_3$	Wavenumber (cm^{-1})	1008	100.00
	Area	7.07	
$0.2B_2O_3$	Wavenumber (cm^{-1})	1012	218.59
	Area	22.52	
$0.4B_2O_3$	Wavenumber (cm^{-1})	1033	248.10
	Area	24.61	
$0.6B_2O_3$	Wavenumber (cm^{-1})	1007	117.73
	Area	15.39	
$0.8B_2O_3$	Wavenumber (cm^{-1})	1006	81.15
	Area	12.81	
$1.0B_2O_3$	Wavenumber (cm^{-1})	1023	N/A
	Area	1.543	

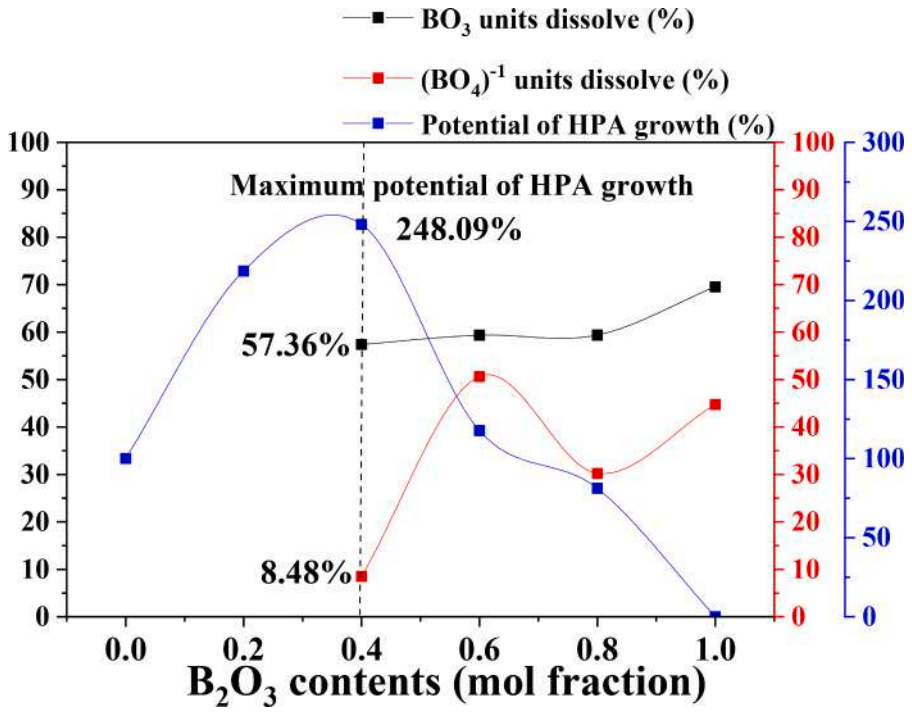

Fig. 11. Percentage of HPA growth and dissolve units of BO_3 and $(BO_4)^{-1}$ within the sample as a function of B_2O_3 molar fraction.

Ethical procedure

- The research meets all applicable standards with regard to the ethics of experimentation and research integrity, and the following is being certified/declared true.
- According to our experience and as along as authors and co-authors for several articles of concerned field, the paper has been submitted with full responsibility, following due ethical procedure, and there is no duplicate publication, fraud, plagiarism, or concerns about animal or human experimentation.

CRediT authorship contribution statement

N.N. Yusof: Conceptualization, Methodology, Software, Formal analysis, Investigation, Resources, Data curation, Validation, Writing – original draft, Writing – review & editing, Visualization. **Siti Maisarah Aziz:** Validation, Supervision, Project administration, Funding acquisition. **F. Mohd Noor:** Conceptualization, Methodology, Software, Resources, Visualization, Supervision, Project administration, Funding acquisition. **S.N. Syed Yaacob:** Methodology, Software, Resources, Validation, Visualization. **S. Hashim:** Supervision, Project administration, Funding acquisition.

Declaration of Competing Interest

None of the authors of this paper has a financial or personal relationship with other people or organizations that could inappropriately influence or bias the content of the paper.

It is to specifically state that "No Competing interests are at stake and there is No Conflict of Interest" with other people or organizations that could inappropriately influence or bias the content of the paper.

Data availability

No data was used for the research described in the article.

Acknowledgments

The authors gratefully acknowledge the financial support from

UniSZA/2020/DPU/05, GUP 15J92, Newton fund 4B456 and UTM through Q. J130000.21A2.05E65.

References

[1] N. Stone-Weiss, H. Bradtmüller, H. Eckert, A. Goel, Composition-structure-solubility relationships in borosilicate glasses: toward a rational design of bioactive glasses with controlled dissolution behavior, ACS Appl. Mater. Interfaces 13 (2021) 31495–31513, https://doi.org/10.1021/acsami.1c07519.

[2] P. Balasubramanian, T. Büttner, V. Miguez Pacheco, A.R. Boccaccini, Boron-containing bioactive glasses in bone and soft tissue engineering, J. Eur. Ceram. Soc. 38 (2018) 855–869, https://doi.org/10.1016/j.jeurceramsoc.2017.11.001.

[3] P. Balasubramanian, L. Hupa, B. Jokic, R. Detsch, A. Grünewald, A.R. Boccaccini, Angiogenic potential of boron-containing bioactive glasses: *in vitro* study, J. Mater. Sci. 52 (2017) 8785–8792, https://doi.org/10.1007/s10853-016-0563-7.

[4] Y. Lin, R.F. Brown, S.B. Jung, D.E. Day, Angiogenic effects of borate glass microfibers in a rodent model, J. Biomed. Mater. Res. Part A 102 (2014) 4491–4499, https://doi.org/10.1002/jbm.a.35120.

[5] M. Hubert, A.J. Faber, On the structural role of boron in borosilicate glasses, Phys. Chem. Glasses 55 (2014) 136–158. Eur. J. Glass Sci. Technol. Part B.

[6] X. Lu, L. Deng, P.H. Kuo, M. Ren, I. Buterbaugh, J. Du, Effects of boron oxide substitution on the structure and bioactivity of SrO-containing bioactive glasses, J. Mater. Sci. 52 (2017) 8793–8811, https://doi.org/10.1007/s10853-017-0836-9.

[7] K. Schuhladen, U. Pantulap, K. Engel, P. Jeleń, Z. Olejniczak, L. Hupa, M. Sitarz, A. R. Boccaccini, Influence of the replacement of silica by boron trioxide on the properties of bioactive glass scaffolds, Int. J. Appl. Glass Sci. 12 (2021) 293–312, https://doi.org/10.1111/ijag.15894.

[8] S. Barheine, S. Hayakawa, C. Jäger, Y. Shirosaki, A. Osaka, Effect of disordered structure of boron-containing calcium phosphates on their *in vitro* biodegradability, J. Am. Ceram. Soc. 94 (2011) 2656–2662, https://doi.org/10.1111/j.1551-2916.2011.04400.x.

[9] R.G. Furlan, W.R. Correr, A.F.C. Russi, M.R. da Costa Iemma, E. Trovatti, É. Pecoraro, Preparation and characterization of boron-based bioglass by sol−gel process, J. Sol Gel Sci. Technol. 88 (2018) 181–191, https://doi.org/10.1007/s10971-018-4806-8.

[10] P. Dey, S.K. Pal, I. Banerjee, R. Sarkar, Effect of addition of B_2O_3 to the sol-gel synthesized 45S5 Bioglass, J. Aust. Ceram. Soc. 56 (2020) 1309–1322, https://doi.org/10.1007/s41779-020-00476-y.

[11] E. Berardo, A. Pedone, P. Ugliengo, M. Corno, DFT modeling of 45S5 and 77S soda-lime phospho-silicate glass surfaces: clues on different bioactivity mechanism, Langmuir 29 (2013) 5749–5759, https://doi.org/10.1021/la304795w.

[12] L.L. Hench, Biomaterials, Science 208 (1980).

[13] G. Malavasi, A. Pedone, M.C. Menziani, Study of the structural role of gallium and aluminum in 45S5 bioactive glasses by molecular dynamics simulations, J. Phys. Chem. B 117 (2013) 4142–4150, https://doi.org/10.1021/jp400721g.

[14] V. Aina, C. Morterra, G. Lusvardi, G. Malavasi, L. Menabue, S. Shruti, C.L. Bianchi, V. Bolis, Ga-modified (Si-Ca-P) sol-gel glasses: possible relationships between surface chemical properties and bioactivity, J. Phys. Chem. C 115 (2011) 22461–22474, https://doi.org/10.1021/jp207217a.

[15] B. Karakuzu-Ikizler, P. Terzioğlu, Y. Basaran-Elalmis, B.S. Tekerek, S. Yücel, Role of magnesium and aluminum substitution on the structural properties and bioactivity of bioglasses synthesized from biogenic silica, Bioact. Mater. 5 (2020) 66–73, https://doi.org/10.1016/j.bioactmat.2019.12.007.

[16] L.L. Hench, J.M Polak, Third-generation biomedical materials, Science 295 (2002) 1014–1017.

[17] N. Stone-Weiss, H. Bradtmüller, M. Fortino, M. Bertani, R.E. Youngman, A. Pedone, H. Eckert, A. Goel, Combined experimental and computational approach toward the structural design of borosilicate-based bioactive glasses, J. Phys. Chem. C 124 (2020) 17655–17674, https://doi.org/10.1021/acs.jpcc.0c04470.

[18] S.A.R. Coelho, J.C. Almeida, I. Unalan, R. Detsch, I.M. Miranda Salvado, A. R. Boccaccini, M.H.V. Fernandes, Cellular response to sol-gel hybrid materials releasing boron and calcium ions, ACS Biomater. Sci. Eng. 7 (2021) 491–506, https://doi.org/10.1021/acsbiomaterials.0c01546.

[19] J. Zhou, H. Wang, S. Zhao, N. Zhou, L. Li, W. Huang, D. Wang, C. Zhang, *In vivo* and *in vitro* studies of borate based glass micro-fibers for dermal repairing, Mater. Sci. Eng. C 60 (2016) 437–445, https://doi.org/10.1016/j.msec.2015.11.068.

[20] A.M. Abdelghany, H. Kamal, Spectroscopic investigation of synergetic bioactivity behavior of some ternary borate glasses containing fluoride anions, Ceram. Int. 40 (2014) 8003–8011, https://doi.org/10.1016/j.ceramint.2013.12.151.

[21] W.C. Lepry, S.N. Nazhat, Highly bioactive sol-gel-derived borate glasses, Chem. Mater. 27 (2015) 4821–4831, https://doi.org/10.1021/acs.chemmater.5b01697.

[22] W.C. Lepry, S. Smith, S.N. Nazhat, Effect of sodium on bioactive sol-gel-derived borate glasses, J. Non Cryst. Solids 500 (2018) 141–148, https://doi.org/10.1016/j.jnoncrysol.2018.07.042.

[23] W. Huang, D.E. Day, K. Kittiratanapiboon, M.N. Rahaman, Kinetics and mechanisms of the conversion of silicate (45S5), borate, and borosilicate glasses to hydroxyapatite in dilute phosphate solutions, J. Mater. Sci. Mater. Med. 17 (2006) 583–596, https://doi.org/10.1007/s10856-006-9220-z.

[24] N. Krishnamacharyulu, G. Jagan Mohini, G. Sahaya Baskaran, V. Ravi Kumar, N. Veeraiah, Investigation on Silver Doped B_2O_3 – SiO_2 – P_2O_5 – Na_2O – CaO Bioglass System for Biomedical Applications, Elsevier B.V., 2018, https://doi.org/10.1016/j.jallcom.2017.10.271.

[25] L.L. Hench, The story of Bioglass®, J. Mater. Sci. Mater. Med. 17 (2006) 967–978, https://doi.org/10.1007/s10856-006-0432-z.

[26] E. Coon, A.M. Whittier, B.M. Abel, E.L. Stapleton, R. Miller, Q. Fu, Viscosity and crystallization of bioactive glasses from 45S5 to 13-93, Int. J. Appl. Glass Sci. 12 (2021) 65–77, https://doi.org/10.1111/ijag.15837.

[27] A. Grandjean, M. Malki, C. Simonnet, D. Manara, B. Penelon, Correlation between electrical conductivity, viscosity, and structure in borosilicate glass-forming melts, Phys. Rev. B Condens. Matter Mater. Phys. 75 (2007), https://doi.org/10.1103/PhysRevB.75.054112.

[28] K.L. Goetschius, The effect of composition on the viscosity, crystallization and dissolution of simple borate glasses and compositional design of borate based bioactive glasses, Doctoral Dissertations, Missouri University of Science and Technology, (2014).

[29] N. Rocton, H. Oudadesse, B. Lefeuvre, H. Peisker, K. Rbii, Fine analysis of interaction mechanism of bioactive glass surface after soaking in SBF solution: AFM and ICP-OES investigations, Appl. Surf. Sci. 505 (2020), 144076,, https://doi.org/10.1016/j.apsusc.2019.144076.

[30] L. Kaewsichan, D. Riyapan, P. Prommajan, J. Kaewsrichan, Effects of sintering temperatures on micro-morphology, mechanical properties, and bioactivity of bone scaffolds containing calcium silicate, ScienceAsia 37 (2011) 240–246, https://doi.org/10.2306/scienceasia1513-1874.2011.37.240.

[31] Y. Yu, Understanding Composition – Structure – Bioactivity Correlations in Bioactive Glasses, Stockholm University, 2018.

[32] W.C. Lepry, S.N. Nazhat, The anomaly in bioactive sol-gel borate glasses, Mater. Adv. 1 (2020) 1371–1381, https://doi.org/10.1039/d0ma00360c.

[33] N. Vedishcheva, Thermodynamic modelling of the structure and properties of glasses in the system Na_2O-B_2O_3-SiO_2 and Na_2O-CaO-SiO_2, in: Proceedings of the 7th European Society of Glass Science and Technology Conference, 2005, pp. 1–7.

[34] D. Ehrt, S. Flügel, Electrical conductivity and viscosity of phosphate glasses and melts, J. Non Cryst. Solids 498 (2018) 461–469, https://doi.org/10.1016/j.jnoncrysol.2018.01.047.

[35] N. Ab Llah, S.B. Jamaludin, Z.C. Daud, M.A.F. Zaludin, Z.A.Z. Jamal, M.S. Idris, R. A.M. Osman, Corrosion behavior of Mg-3Zn/bioglass (45S5) composite in simulated body fluid (SBF) and phosphate buffered saline (PBS) solution, AIP Conf. Proc. 1756 (2016), https://doi.org/10.1063/1.4958753.

[36] M. Cerruti, D. Greenspan, K. Powers, Effect of pH and ionic strength on the reactivity of Bioglass® 45S5, Biomaterials 26 (2005) 1665–1674, https://doi.org/10.1016/j.biomaterials.2004.07.009.

[37] S. Höhn, K. Zheng, S. Romeis, M. Brehl, W. Peukert, D. de Ligny, S. Virtanen, A. R. Boccaccini, Effects of medium pH and preconditioning treatment on protein adsorption on 45S5 bioactive glass surfaces, Adv. Mater. Interfaces 7 (2020), https://doi.org/10.1002/admi.202000420.

[38] A. El-Ghannam, P. Ducheyne, I.M. Shapiro, Porous bioactive glass and hydroxyapatite ceramic affect bone cell function *in vitro* along different time lines, J. Biomed. Mater. Res. 36 (1997) 167–180, https://doi.org/10.1002/(SICI)1097-4636(199708)36:2<167::AID-JBM5>3.0.CO;2-I.

[39] E. Vafa, R. Bazargan-Lari, M.E. Bahrololoom, Synthesis of 45S5 bioactive glass-ceramic using the sol-gel method, catalyzed by low concentration acetic acid extracted from homemade vinegar, J. Mater. Res. Technol. 10 (2021) 1427–1436, https://doi.org/10.1016/j.jmrt.2020.12.093.

[40] L. Souza, J.H. Lopes, D. Encarnação, I.O. Mazali, R.A. Martin, J.A. Camilli, C. A. Bertran, Comprehensive *in vitro* and *in vivo* studies of novel melt-derived Nb-substituted 45S5 Bioglass reveal its enhanced bioactive properties for bone healing, Sci. Rep. 8 (2018) 1–15, https://doi.org/10.1038/s41598-018-31114-0.

[41] M. Arango-Ospina, L. Hupa, A.R. Boccaccini, Bioactivity and dissolution behavior of boron-containing bioactive glasses under static and dynamic conditions in different media, Biomed. Glasses 5 (2019) 124–139, https://doi.org/10.1515/bglass-2019-0011.

[42] H.B. Pan, X.L. Zhao, X. Zhang, K.B. Zhang, L.C. Li, Z.Y. Li, W.M. Lam, W.W. Lu, D. P. Wang, W.H. Huang, K.L. Lin, J. Chang, Strontium borate glass: potential biomaterial for bone regeneration, J. R. Soc. Interface 7 (2010) 1025–1031, https://doi.org/10.1098/rsif.2009.0504.

[43] X. Liu, H. Pan, H. Fu, Q. Fu, M.N. Rahaman, W. Huang, Conversion of borate-based glass scaffold to hydroxyapatite in a dilute phosphate solution, Biomed. Mater. 5 (2010), https://doi.org/10.1088/1748-6041/5/1/015005.

[44] H. Liu, H. Yazici, C. Ergun, T.J. Webster, H. Bermek, An *in vitro* evaluation of the Ca/P ratio for the cytocompatibility of nano-to-micron particulate calcium phosphates for bone regeneration, Acta Biomater. 4 (2008) 1472–1479, https://doi.org/10.1016/j.actbio.2008.02.025.

[45] M. Araújo, M. Miola, G. Baldi, J. Perez, E. Verné, Bioactive glasses with low Ca/P ratio and enhanced bioactivity, Materials 9 (2016), https://doi.org/10.3390/ma9040226.

[46] V. Stanić, Boron-containing bioactive glasses for bone regeneration, 2019th ed., WoodHead Publishing, United Kingdom, 2018. doi:10.1016/B978-0-08-102196-5.00008-2.

[47] X. Kesse, C. Vichery, A. Jacobs, S. Descamps, J.M. Nedelec, Unravelling the impact of calcium content on the bioactivity of sol-gel-derived bioactive glass nanoparticles, ACS Appl. Bio Mater. 3 (2020) 1312–1320, https://doi.org/10.1021/acsabm.0c00036.

[48] M.N. Rahaman, D.E. Day, B. Sonny Bal, Q. Fu, S.B. Jung, L.F. Bonewald, A. P. Tomsia, Bioactive glass in tissue engineering, Acta Biomater. 7 (2011) 2355–2373, https://doi.org/10.1016/j.actbio.2011.03.016.

[49] A.R. Barron, C. Smith, C.E. Hamilton, Chemistry of the main group elements, Inorg. Chem. (2015) 225–238. https://cnx.org/contents/9G6Gee4A@25.9:HUxicYBD@1/Preface-to-the-Chemistry-of-the-Main-Group-Elements.

[50] B.C. Bunker, Molecular mechanisms for corrosion of silica and silicate glasses, J. Non Cryst. Solids 179 (1994) 300–308, https://doi.org/10.1016/0022-3093(94)90708-0.

[51] J. Ning, A. Yao, D. Wang, W. Huang, H. Fu, X. Liu, X. Jiang, X. Zhang, Synthesis and *in vitro* bioactivity of a borate-based bioglass, Mater. Lett. 61 (2007) 5223–5226, https://doi.org/10.1016/j.matlet.2007.04.089.
[52] M. Fournier, A. Ull, E. Nicoleau, Y. Inagaki, M. Odorico, P. Frugier, S. Gin, Glass dissolution rate measurement and calculation revisited, J. Nucl. Mater. 476 (2016) 140–154, https://doi.org/10.1016/j.jnucmat.2016.04.028.
[53] J.D. Vienna, J.J. Neeway, J.V. Ryan, S.N. Kerisit, Impacts of glass composition, pH, and temperature on glass forward dissolution rate, npj Mater. Degrad. 2 (2018) 1–12, https://doi.org/10.1038/s41529-018-0042-5.
[54] Y. Yu, B. Stevensson, M. Edén, Medium-range structural organization of phosphorus-bearing borosilicate glasses revealed by advanced solid-state NMR experiments and MD simulations: consequences of B/Si substitutions, J. Phys. Chem. B 121 (2017) 9737–9752, https://doi.org/10.1021/acs.jpcb.7b06654.
[55] L. Bingel, D. Groh, N. Karpukhina, D.S. Brauer, Influence of dissolution medium pH on ion release and apatite formation of Bioglass® 45S5, Mater. Lett. 143 (2015) 279–282, https://doi.org/10.1016/j.matlet.2014.12.124.
[56] T.G.V.M. Rao, A. Rupesh Kumar, K. Neeraja, N. Veeraiah, M. Rami Reddy, Optical and structural investigation of Eu^{3+} ions in Nd^{3+} co-doped magnesium lead borosilicate glasses, J. Alloy. Compd. 557 (2013) 209–217, https://doi.org/10.1016/j.jallcom.2012.12.162.
[57] G. Shao, X. Wu, Y. Kong, S. Cui, X. Shen, C. Jiao, J. Jiao, Thermal shock behavior and infrared radiation property of integrative insulations consisting of $MoSi_2$/borosilicate glass coating and fibrous ZrO_2 ceramic substrate, Surf. Coat. Technol. 270 (2015) 154–163, https://doi.org/10.1016/j.surfcoat.2015.03.008.
[58] M. Schumacher, P. Habibovic, S. van Rijt, Mesoporous bioactive glass composition effects on degradation and bioactivity, Bioact. Mater. 6 (2021) 1921–1931, https://doi.org/10.1016/j.bioactmat.2020.12.007.
[59] V. Aina, F. Bonino, C. Morterra, M. Miola, C.L. Bianchi, G. Malavasi, M. Marchetti, V. Bolis, Influence of the chemical composition on nature and activity of the surface layer of Zn-substituted sol-gel (bioactive) glasses, J. Phys. Chem. C 115 (2011) 2196–2210, https://doi.org/10.1021/jp1101708.
[60] A.L.B. Maçon, T.B. Kim, E.M. Valliant, K. Goetschius, R.K. Brow, D.E. Day, A. Hoppe, A.R. Boccaccini, I.Y. Kim, C. Ohtsuki, T. Kokubo, A. Osaka, M. Vallet-Regí, D. Arcos, L. Fraile, A.J. Salinas, A.V. Teixeira, Y. Vueva, R.M. Almeida, M. Miola, C. Vitale-Brovarone, E. Verné, W. Höland, J.R. Jones, A unified *in vitro* evaluation for apatite-forming ability of bioactive glasses and their variants, J. Mater. Sci. Mater. Med. 26 (2015) 1–10, https://doi.org/10.1007/s10856-015-5403-9.
[61] R. Chen, Q. Li, Q. Zhang, S. Xu, J. Han, P. Huang, Z. Yu, D. Jia, J. Liu, H. Jia, M. Shen, B. Hu, H. Wang, H. Zhan, T. Zhang, K. Ma, J. Wang, Nanosized HCA-coated borate bioactive glass with improved wound healing effects on rodent model, Chem. Eng. J. 426 (2021), 130299, https://doi.org/10.1016/j.cej.2021.130299.
[62] D. Cheng, D. Liu, T. Tang, X. Zhang, X. Jia, Q. Cai, X. Yang, Effects of Ca/P molar ratios on regulating biological functions of hybridized carbon nanofibers containing bioactive glass nanoparticles, Biomed. Mater. 12 (2017), https://doi.org/10.1088/1748-605X/aa6521 (Bristol).
[63] J. Faure, R. Drevet, A. Lemelle, N. Ben Jaber, A. Tara, H. El Btaouri, H. Benhayoune, A new sol-gel synthesis of 45S5 bioactive glass using an organic acid as catalyst, Mater. Sci. Eng. C 47 (2015) 407–412, https://doi.org/10.1016/j.msec.2014.11.045.
[64] A.K. Yadav, P. Singh, A Review of Structure of Oxide Glasses by Raman Spectroscopy, R. Soc. Chem. (2012) 11002–11003, https://doi.org/10.1039/C5RA13043C.
[65] M. Ouis, A. Abdelghany, H. Elbatal, Corrosion mechanism and bioactivity of borate glasses analogue to Hench's bioglass, Process. Appl. Ceram. 6 (2012) 141–149, https://doi.org/10.2298/pac1203141o.
[66] R.A. Youness, M.A. Taha, M. Ibrahim, A. El-Kheshen, FTIR spectral characterization, mechanical properties and antimicrobial properties of La-doped phosphate-based bioactive glasses, Silicon 10 (2018) 1151–1159, https://doi.org/10.1007/s12633-017-9587-0.
[67] L. de Siqueira, T.M.B. Campos, S.E.A. Camargo, G.P. Thim, E.S. Trichês, Structural, crystallization and cytocompatibility evaluation of the 45S5 Bioglass-derived glass-ceramic containing niobium, J. Non Cryst. Solids 555 (2021) 1–8, https://doi.org/10.1016/j.jnoncrysol.2020.120629.
[68] G. Taveri, O. Hanzel, J. Sedláček, J. Toušek, Z. Neščaková, M. Michálek, I. Dlouhý, M. Hnatko, Consolidation of Bioglass® 45S5 suspension through cold isostatic pressing, Ceram. Int. 47 (2021) 4090–4096, https://doi.org/10.1016/j.ceramint.2020.09.283.
[69] M.R. Ahmed, M. Shareefuddin, EPR, optical, physical and structural studies of strontium alumino-borate glasses containing Cu^{2+} ions, SN Appl. Sci. 1 (2019) 1–10, https://doi.org/10.1007/s42452-019-0201-5.
[70] L.A. Adams, E.R. Essien, A.T. Adesalu, M.L. Julius, Bioactive glass 45S5 from diatom biosilica, J. Sci. Adv. Mater. Dev. 2 (2017) 476–482, https://doi.org/10.1016/j.jsamd.2017.09.002.
[71] J.L. Ryszkowska, M. Auguścik, A. Sheikh, A.R. Boccaccini, Biodegradable polyurethane composite scaffolds containing Bioglass® for bone tissue engineering, Compos. Sci. Technol. 70 (2010) 1894–1908, https://doi.org/10.1016/j.compscitech.2010.05.011.
[72] J.S. Fernandes, P. Gentile, R. Moorehead, A. Crawford, C.A. Miller, R.A. Pires, P. V. Hatton, R.L. Reis, Design and properties of novel substituted borosilicate bioactive glasses and their glass-ceramic derivatives, Cryst. Growth Des. 16 (2016) 3731–3740, https://doi.org/10.1021/acs.cgd.6b00231.
[73] J.L. George, R.K. Brow, *In-situ* characterization of borate glass dissolution kinetics by μ-Raman spectroscopy, J. Non Cryst. Solids 426 (2015) 116–124, https://doi.org/10.1016/j.jnoncrysol.2015.07.003.